Supplementary Information

Effective 3D open-channel nanostructures of a $MgMn_2O_4$ positive electrode for rechargeable Mg batteries operated at room temperature

Kazuki Sone,[a] Yoshihiro Hayashi,[a] Toshihiko Mandai,[b] Shunsuke Yagi,[b] Yuya Oaki,[a] and Hiroaki Imai*[a]

[a]Department of Applied Chemistry, Faculty of Science and Technology, Keio University, 3-14-1 Hiyoshi, Kohoku-ku, Yokohama 223-8522, Japan

[b]Center for Research on Energy and Environmental Materials, National Institute for Materials Science (NIMS), 1-1 Namiki, Tsukuba, 305-0044 Ibaraki, Japan.

[c]Institute of Industrial Science, The University of Tokyo, 4-6-1 Komaba, Meguro-ku, Tokyo 153-8505, Japan.

Fig. S1 Illustrations of the MMO powder preparation using a modified sol–gel method through propylene-oxide-driven complex polymerization, in which supersonic was irradiated to accelerate the gelation and the gel-aging time was controlled.

Fig. S2 The Mg coin-cell structure and the components inside: (a) the cross-sectional illustration of the coin cell, and the structural specifications for (b) the full cell with the MMO positive electrode and the Mg negative one in the $Mg[B(HFIP)_4]_2$/G3 electrolyte, and the half cells with the MMO positive electrode and the carbon negative one in (c) the $Mg[B(HFIP)_4]_2$/G3 electrolyte and (d) the $Mg(ClO_4)_2$ /AN electrolyte.

Fig. S3 Cyclic voltammograms for the $Mg(ClO_4)_2$/AN electrolyte using the $MgMn_2O_4$ positive electrode with and without the V_2O_5 coating.

Fig. S4 Current-voltage characteristics for the $Mg[B(HFIP)_4]_2$/G3 electrolyte (a) and the cyclic voltammogram of the Mg/(borate/G3)/MMO system (b).

Fig. S5 Pore-size distributions, cumulative pore volumes, and S_{BET} measured by the nitrogen adsorption isotherm for the MMO powders obtained by 5 h-calcination at 300 °C from the dried gels aged for (1) 1 h, (b) 24 h, (c) 72 h, and (d) 168 h.

Fig. S6 TG/DTA profiles of the dried gel.

Fig. S7 Pore-size distributions, cumulative pore volumes, and S_{BET} measured by the nitrogen adsorption isotherm for the MMO powders obtained by the 5 h calcination at (a) 300 °C (b) 400 °C (c) 500 °C, and (d) 600 °C. All of the gels were aged for 24 h.

Fig. S8 Arrhenius plot of S_{BET} and D_{BET} for the MMO powders obtained by the 5 h calcination at 300 –600 °C from the dried gels aged for 24 h.

Fig. S9 Open circuit voltage (OCV) and the average discharged potentials at 25 °C in the 1st cycle for the full cell of Mg/(borate/G3)/MMO as a function of S_{BET} of the MMO powders.

Fig. S10 Discharge capacity at 25 °C in the 1st cycle for the full cell of Mg/(borate/G3)/MMO as a function of D_{BET} of the MMO powders.

Fig. S11 Discharge capacities as a function of the maximum charging voltage in the full cell of the Mg/(borate/G3)/MMO, in which was used the MMO powder calcinated at 300 °C from the 1 h-aged gel.

Fig. S12 Photographs of (a) the Mg-alloy negative electrode and (b) the separator in the full cell of Mg/(borate/G3)/MMO before and after the 10 cycle operation.

Fig. S13 Changes in the XRD patterns of the MMO powders (a) in the half cell, Mg/(perchlorate/AN)/MMO, cycled with ΔE = 2.0V (-1.0–+1.0V vs. CE, or eq. +1.6–+3.6 V vs. Mg/Mg^{2+}) and (b) in the full cell, Mg/(borate/G3)/MMO, cycled in ΔE = 3.8 V (+0.2–+4.0 V vs. Mg/Mg^{2+}) .

Fig. S14 Cyclic voltammograms for the Mg/($[B(HFIP)_4]_2$/G3)/MMO having low (108 m^2/g) (a) and high (246 m^2/g) (b) specific surface areas

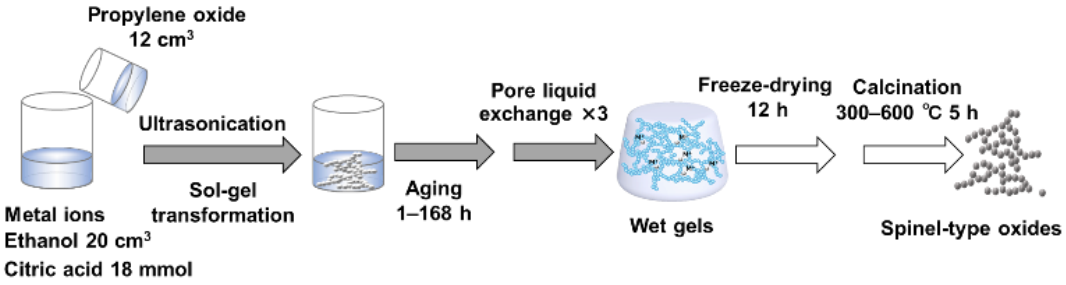

Fig. S1 Illustrations of the MMO powder preparation using a modified sol–gel method through propylene-oxide-driven complex polymerization, in which supersonic was irradiated to accelerate the gelation and the gel-aging time was controlled.

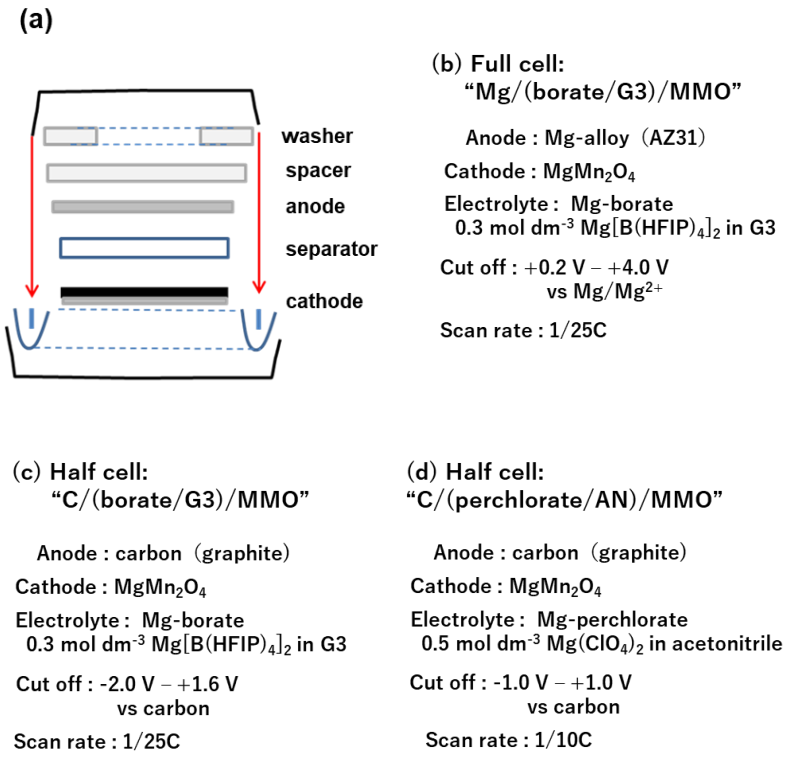

Fig. S2 The Mg coin-cell structure and the components inside: (a) the cross-sectional illustration of the coin cell, and the structural specifications for (b) the full cell with the MMO positive electrode and the Mg-alloy negative one in the $Mg[B(HFIP)_4]_2$/G3 electrolyte, and the half cells with the MMO positive electrode and the carbon negative one in (c) the $Mg[B(HFIP)_4]_2$/G3 electrolyte and (d) the $Mg(ClO_4)_2$ /AN electrolyte.

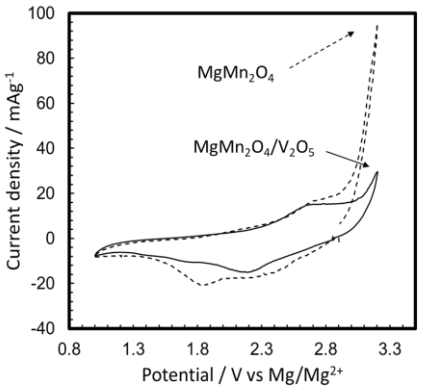

Fig. S3 Cyclic voltammograms for the $Mg(ClO_4)_2$/AN electrolyte using the $MgMn_2O_4$ positive electrode with and without the V_2O_5 coating. Carbon was used as a counter electrode. A Ag wire immersed in AN containing 0.01 mol/dm^3 $AgNO_3$ and 0.10 mol/dm^3 tetrabutylammonium perchlorate was used as the reference electrode. The measured potentials were converted to their values vs. Mg/Mg^{2+} using the following relationship: 0 V vs. Mg/Mg^{2+} = –2.6 V vs. Ag/Ag^+.

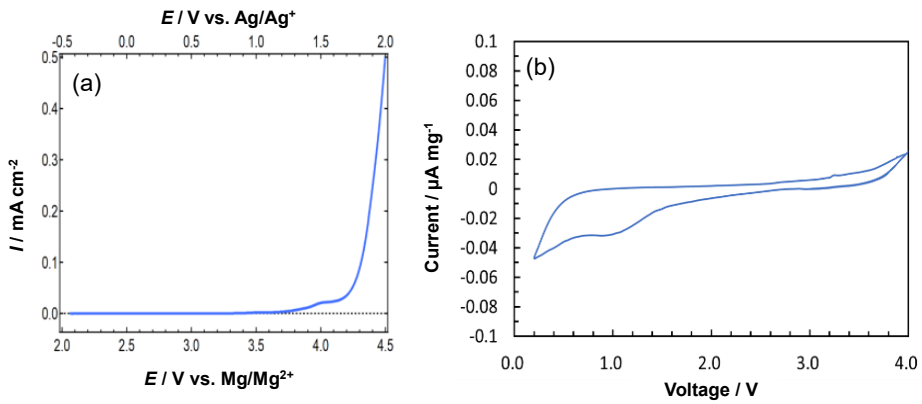

Fig. S4 Current-voltage characteristics for the $Mg[B(HFIP)_4]_2$/G3 electrolyte (a) and the cyclic voltammogram of the Mg/(borate/G3)/MMO system (b). The specific surface area of the MMO powder was 42 m^2/g.

We measured cyclic voltammograms (Fig. S3) for the $Mg(ClO_4)_2$/AN electrolyte using the MMO positive electrode with and without the V_2O_5 coating. As shown in the voltammograms, anodic electrolyte decomposition occurred above about 2.8 V vs Mg/Mg^{2+}. Although the V_2O_5 coating on the MMO positive electrode was reported to suppress the decomposition of the electrolyte (Ref. 23 in the main manuscript), we observed the anodic decomposition above about 3.0 V vs Mg/Mg^{2+}. The anodic current hinders the oxidation of the positive electrode and results in the lower performance of the MMO powders. On the other hand, the anodic decomposition of the $Mg[B(HFIP)_4]_2$/G3 electrolyte occurs above 4.0 V vs Mg/Mg^{2+} as shown in Fig. S4. Thus, the cutoff voltage was limited between –1.0 V and +1.0 V vs. carbon for the $Mg(ClO_4)_2$/AN electrolyte and was set between –2.0 V and +1.6 V vs. carbon for the $Mg[B(HFIP)_4]_2$/G3 electrolyte.

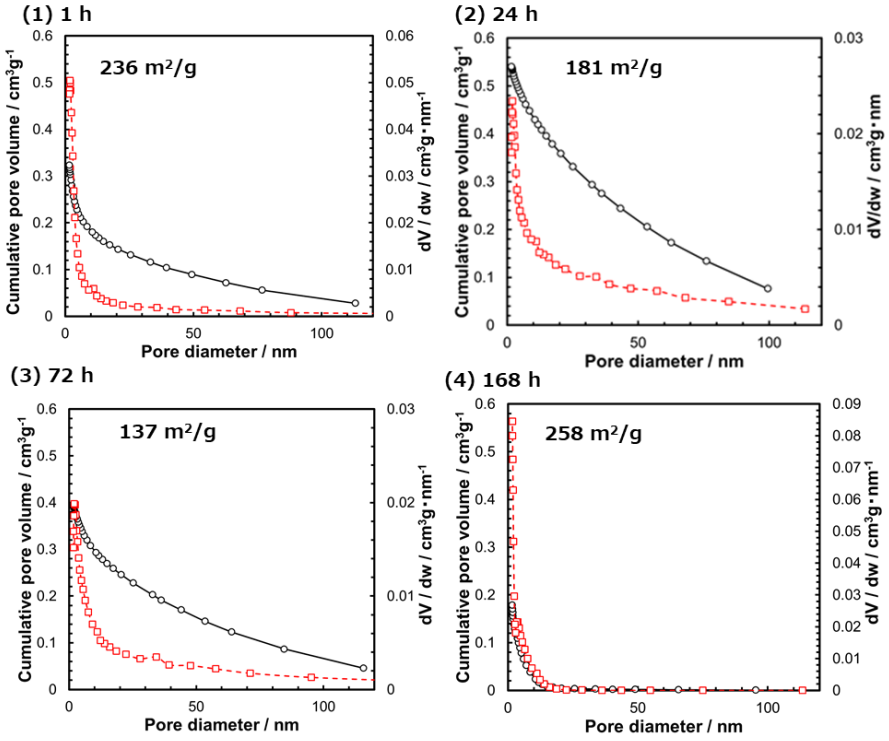

Fig. S5 Pore-size distributions, cumulative pore volumes, and S_{BET} measured by the nitrogen adsorption isotherm for the MMO powders obtained by 5 h calcination at 300 °C from the dried gels aged for (1) 1 h, (b) 24 h, (c) 72 h, and (d) 168 h.

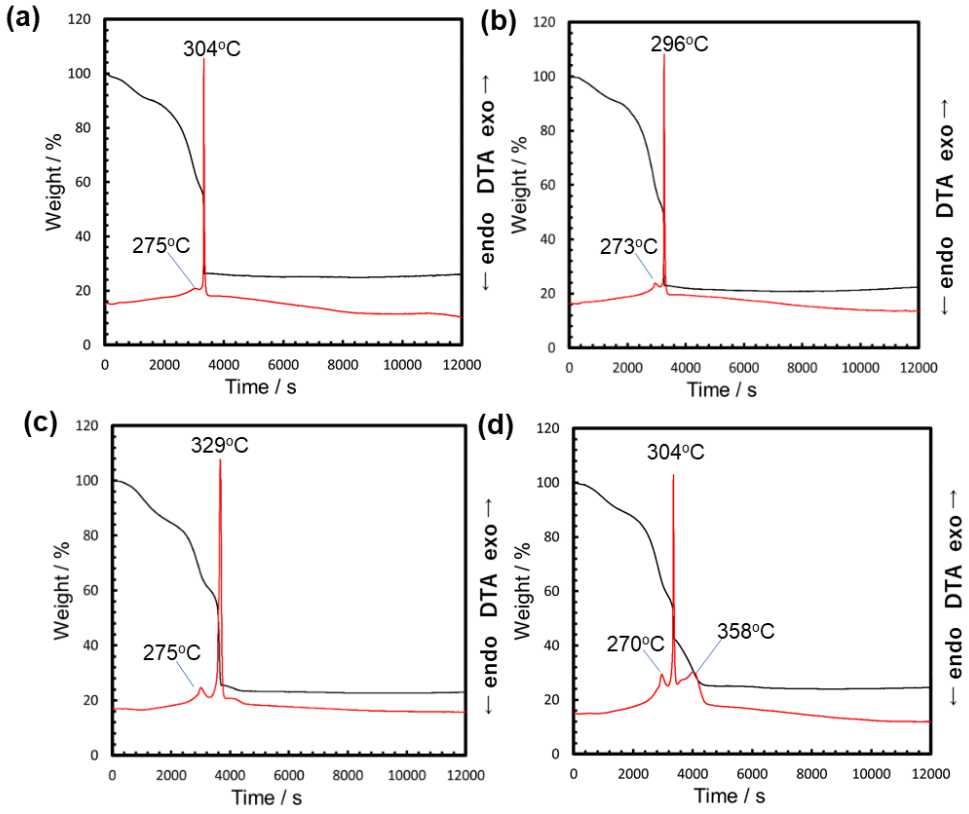

Fig. S6 TG/DTA profiles of the dried gel aged for (a) 1h, (b) 24 h, (c) 72 h, and (d) 168 h. The temperature rising rate was 5 °C/min.

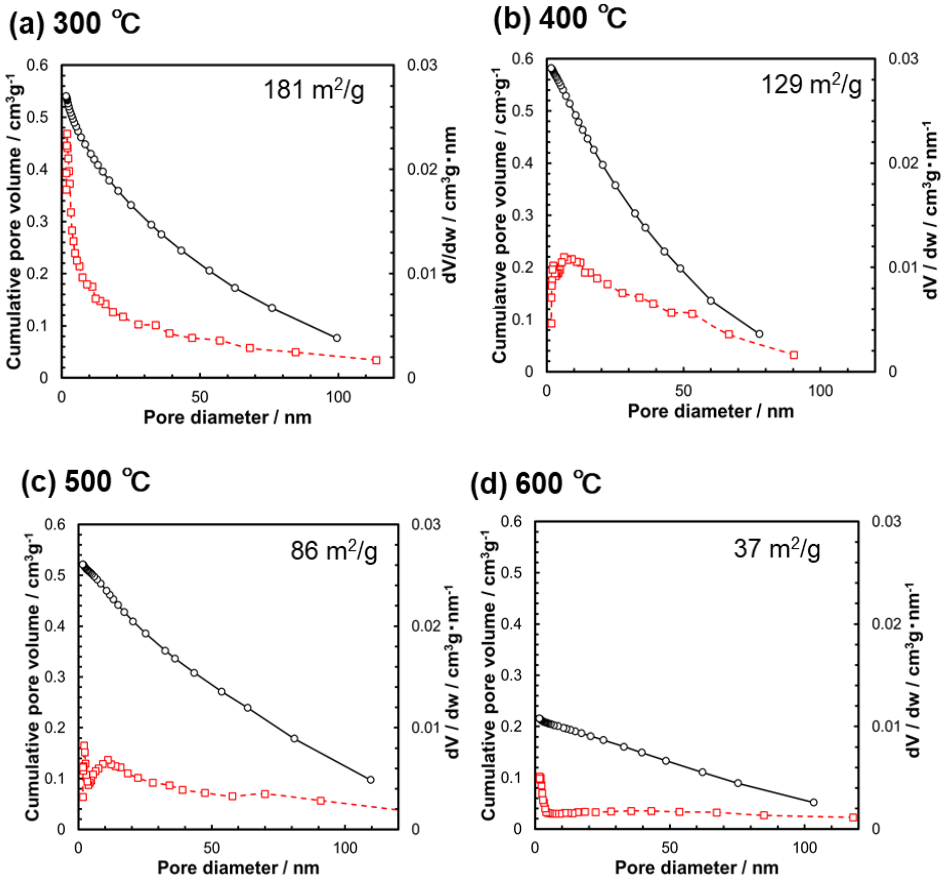

Fig. S7 Pore-size distributions, cumulative pore volumes, and S_{BET} measured by the nitrogen adsorption isotherm for the MMO powders obtained by the 5 h calcination at (a) 300 °C (b) 400 °C (c) 500 °C, and (d) 600 °C. All of the gels were aged for 24 h.

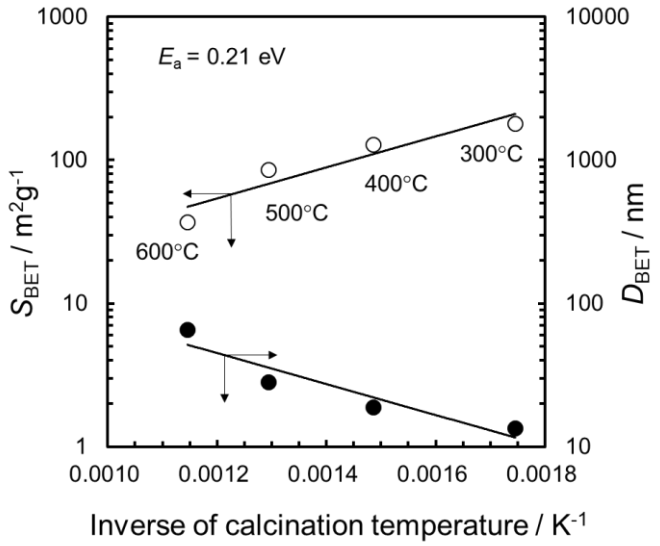

Fig. S8 Arrhenius plot of S_{BET} and D_{BET} for the MMO powders obtained by the 5 h-calcination at 300–600°C from the dried gels aged for 24 h.

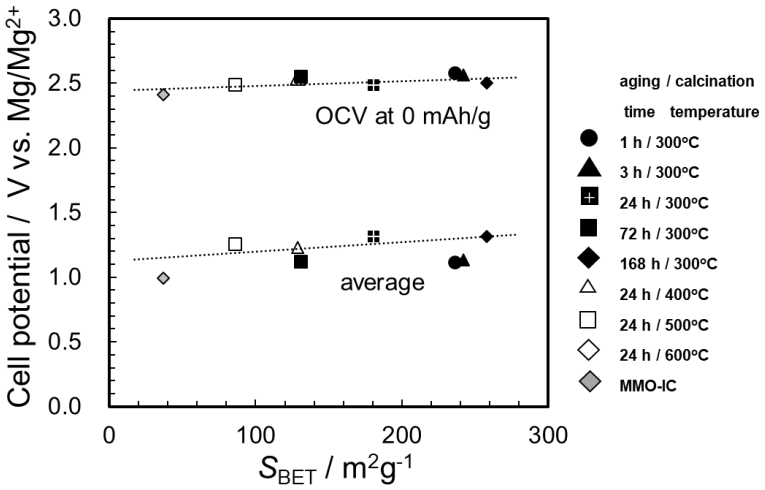

Fig. S9 Open circuit voltage (OCV) and the average discharged potentials at 25 °C in the 1st cycle for the full cell of Mg/(borate/G3)/MMO as a function of S_{BET} of the MMO powders in the positive electrodes.

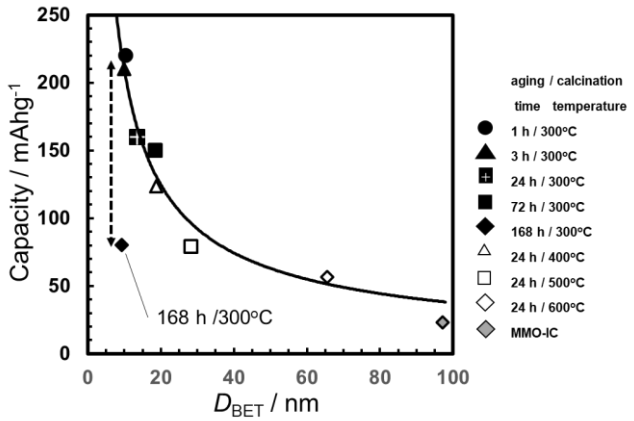

Fig. S10 Discharge capacity at 25 °C in the 1st cycle for the full cell of Mg/(borate/G3)/MMO as a function of D_{BET} of the MMO powders

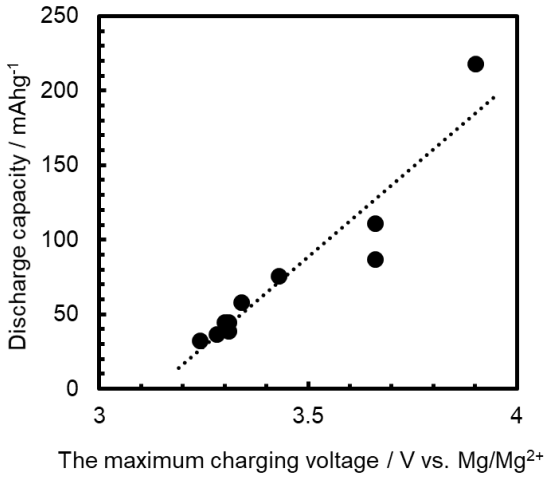

Fig. S11 Discharge capacities as a function of the maximum charging voltage in the full cell of the Mg/(borete/G3)/MMO, in which was used the MMO powder calcinated at 300 °C from the 1 h aged gel.

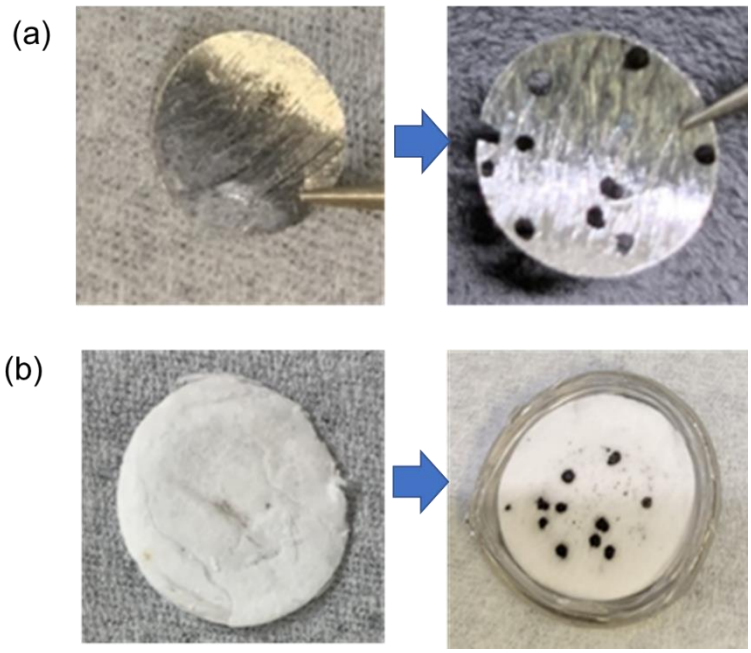

Fig. S12 Photographs of (a) the Mg-alloy negative electrode and (b) the separator in the full cell of Mg/(borate/G3)/MMO before and after the 10 cycle operation.

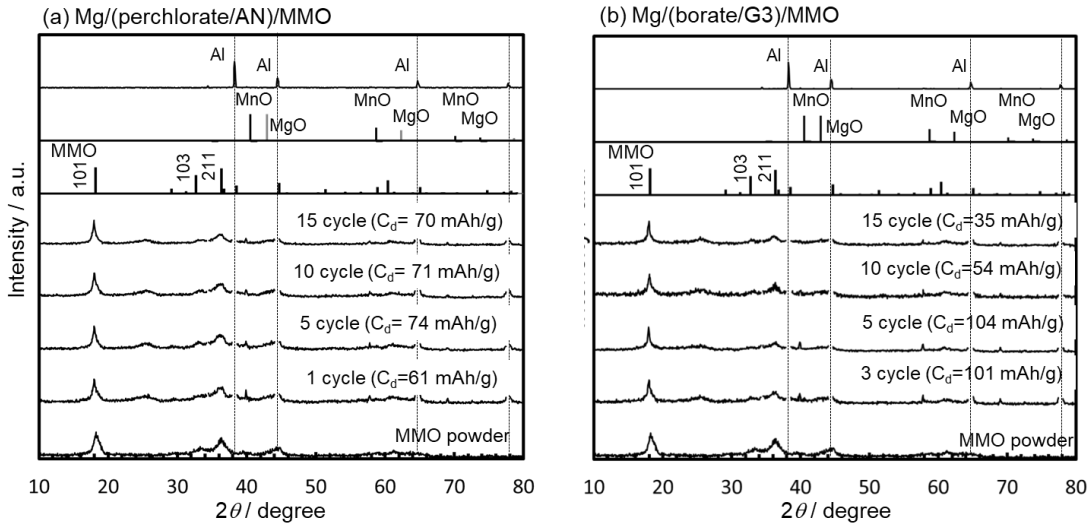

Fig. S13 Changes in the XRD patterns of the MMO powders (a) in the half cell, Mg/(perchlorate/AN)/MMO, cycled on ΔE = 2.0 V (-1.0– +1.0 V vs. CE, or eq. +1.6–+3.6 V vs. Mg/Mg^{2+}) and (b) in the full cell, Mg/(borate/G3)/MMO, cycled in ΔE = 3.8 V (+0.2–+4.0 V vs. Mg/Mg^{2+}) .

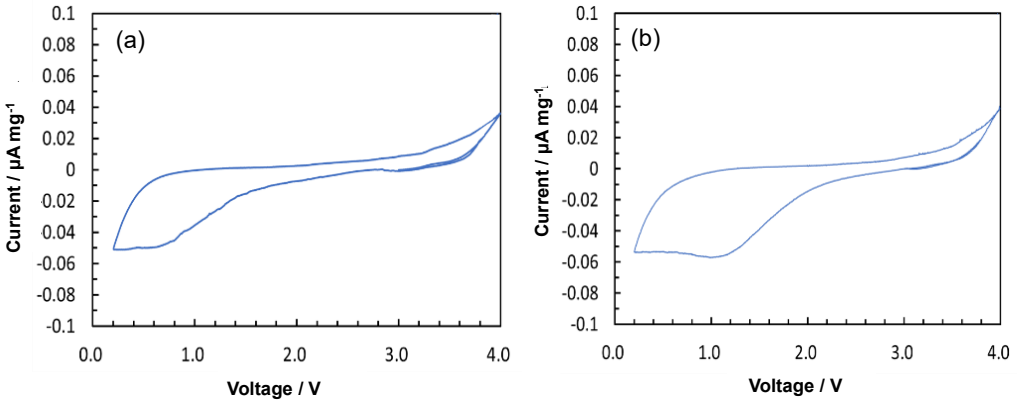

Fig. S14 Cyclic voltammograms for the Mg/([B(HFIP)$_4$]$_2$/G3)/MMO having low (108 m^2/g) (a) and high (246 m^2/g) (b) specific surface areas